Fragmented superradiance of a Bose-Einstein condensate in an optical cavity

Axel U. J. Lode* and Christoph Bruder

Department of Physics, University of Basel, Klingelbergstrasse 82, CH-4056 Basel, Switzerland

The Dicke model and the superradiance of two-level systems in a radiation field have many applications. Recently, a Dicke quantum phase transition has been realized with a Bose-Einstein condensate in a cavity. We numerically solve the many-body Schrödinger equation and study correlations in the ground state of interacting bosons in a cavity as a function of the strength of a driving laser. Beyond a critical strength, the bosons occupy multiple modes macroscopically while remaining superradiant. This fragmented superradiance can be detected by analyzing the variance of single-shot measurements.

The Dicke quantum phase transition from a normal to a superradiant state is driven by the cooperativity of the emitters in a light field [1–4]. It has recently been realized and studied in a number of different systems like superconducting qubits coupled to resonators [5–7], electromagnetically coupled quantum dots [9], the magnetoresistance of organic light-emitting diodes [10], a plasma of Helium atoms [11], a superradiant laser [12], and a Bose-Einstein condensate in an optical cavity [13–17]. All of these systems are formed of constituents which are more complex than the two-level emitters considered in the Dicke model which makes its successful application to these systems even more remarkable.

The unique experimental control of Bose-Einstein condensates of ultracold atoms [18–20] has made them versatile quantum simulators for other systems, like here, the Dicke Hamiltonian [13–16]. Bose-Einstein condensates or ultracold Fermi gases, however, cannot generally be described within a two-level framework since they constitute many-body systems of interacting atoms [21–24]. In many-body systems, correlations arise due to the interactions between the particles and hence two-level descriptions [25, 26] or mean-field approaches [27–29] might fail to accurately describe them [23, 24, 30]. One striking example for a correlation effect not captured by mean-field methods is the emergence of fragmentation [31–33] in interacting Bose-Einstein condensed systems: the reduced one-body density matrix starts to have more than one macroscopic eigenvalue.

In this paper, we will focus on a Bose-Einstein condensate in an optical cavity and show how the fact that the Bose-Einstein condensate is an interacting many-body system and not just an ensemble of two-level systems substantially enriches the phase diagram beyond the Dicke model. Our focus here is on the emergent phases triggered by interactions in a zero-temperature system. The phase diagram of the noninteracting system at finite temperature (the Dicke-Hepp-Lieb phase transition) is discussed in Ref. [34].

In the following, we apply a numerical many-body approach for ultracold atoms in multimodal cavities and demonstrate that their ground state in a single-mode cavity exhibits correlations that indicate the fragmen-
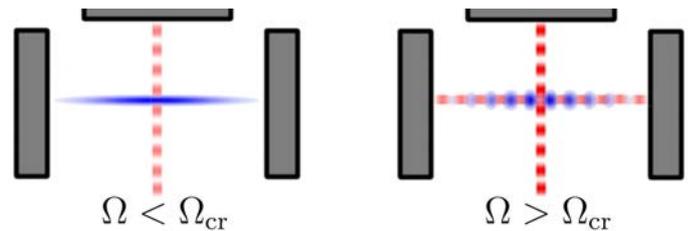

FIG. 1. Setup for the Dicke quantum phase transition with a Bose-Einstein condensate in an optical cavity. For a cavity pump power Ω that is smaller than the critical pump power Ω_{cr}, the Bose-Einstein condensate (blue) in the cavity formed by the left and right mirrors (gray) is unaffected by the pump laser and no population of cavity photons (red) is built up (left panel). For pump powers Ω larger than the critical value Ω_{cr}, the Bose-Einstein condensate self-organizes as a consequence of the potential which is built up by the population of the cavity with photons (right panel).

tation of the system. For sufficient pump power, the system enters a state of *fragmented superradiance*. The pump power needed to trigger the emergence of correlations in the ground state of the atoms is generally larger than the pump power necessary to enter the superradiant state. The existence of this third phase modifies the phase diagram of ultracold bosons in an optical cavity and demonstrates the limitations of the mapping of the system to the Dicke model which exhibits only two phases for bosons in single-mode cavities.

The realization of the Dicke quantum phase transition with a Bose-Einstein condensate in a single-mode optical cavity in [13–16] motivates us to study the role of correlations in the process of self-organization. To proceed, we investigate the ground state of a system of $N = 100$ interacting bosonic atoms in a single-mode cavity as a function of the pump rate, see Fig. 1 for a scheme of the system.

The bosons are governed by the time-dependent many-body Schrödinger equation $i\partial_t|\Psi\rangle = H|\Psi\rangle$ with the Hamiltonian

$$H = \sum_{i=1}^{N}[T_{\mathbf{r}_i} + V(\mathbf{r}_i)] + \lambda_0 \sum_{i>j=1}^{N}\delta(\mathbf{r}_i, \mathbf{r}_j). \quad (1)$$

Here, $T_{\mathbf{r}_i}$ is the kinetic energy of the i-th atom, $V(\mathbf{r}) = V_{1\text{-body}}(\mathbf{r}) + V_{\text{cavity}}(\mathbf{r})$ is a one-particle potential that contains the external trapping $V_{1\text{-body}}$ of the atoms and the potential V_{cavity} generated by the photons in the cavity and pump laser beam (see right panel of Fig. 1). The terms proportional to λ_0 generate a repulsive contact interaction. We choose $\lambda_0 = 0.01$ for the interaction strength λ_0 which is proportional to the s-wave scattering length and adjustable in experiment (see Ref. [35] for experimental parameters to realize this choice for λ_0). The potential $V_{\text{cavity}}(\mathbf{r})$ is a function of the cavity field amplitude α, which is in turn obtained from the equation of motion of the cavity [29, 37],

$$i\partial_t \alpha(t) = \left[-\Delta_c + \sum_{k,q=1}^{M} \rho_{kq}(t) U_{kq}^d - i\kappa \right] \alpha(t)$$
$$+ \sum_{k,q=1}^{M} \rho_{kq}(t) \eta_{kq}^d(t) . \quad (2)$$

Here, we used $\langle \Psi(t) | U(\mathbf{r}) | \Psi(t) \rangle = \sum_{k,q=1}^{M} \rho_{kq}(t) U_{kq}$ and $\langle \Psi(t) | \eta(\mathbf{r},t) | \Psi(t) \rangle = \sum_{k,q=1}^{M} \rho_{kq}(t) \eta_{kq}(t)$, where $U(\mathbf{r})$ and $\eta(\mathbf{r},t)$ are proportional to the cavity mode and pump laser profiles, and ρ_{kq} are the matrix elements of the reduced one-body density matrix that is normalized to N, see [37]. The cavity is detuned by Δ_c from the atomic resonance and its loss rate is given by κ. We employ the time-dependent multiconfigurational Hartree method for indistinguishable particles (MCTDH-X) to compute the ground state of the many-body system coupled to the equation of motion of the cavity amplitude, see Supplementary Material [37] as well as Refs. [23, 43, 44] for details.

In the following we will consider a one-dimensional setup, i.e., a collinear arrangement of the pump laser and the trapped atoms, and use the coordinate x instead of $\mathbf{r}$. We assume the external confinement to be harmonic, $V_{1\text{-body}}(x) = \frac{1}{2}x^2$ and choose dimensionless units [35] and cavity parameters [37, 45]. The potential exerted on the bosons by the photons in the pump laser and the cavity [13, 37] is given by

$$V_{\text{cavity}}(x) = |\alpha|^2 U_0 \cos^2(kx) + (\alpha + \alpha^*)\eta \cos(kx) . \quad (3)$$

Here, the terms proportional to U_0 and η refer to the cavity photons and the pump laser, respectively, see Eq. (2) and Supplementary Material [37].

Since our system is one-dimensional and parabolically confined, we expect to discover physics different from previous investigations in two-dimensional systems in a lattice, where superfluid self-organized and Mott-insulator self-organized [46] as well as supersolid and charge-density wave [47, 48] phases have been demonstrated.

As a first step in our investigation, we show the density $\rho(x)$ and the one-body potential $V(x)$ of the ground state
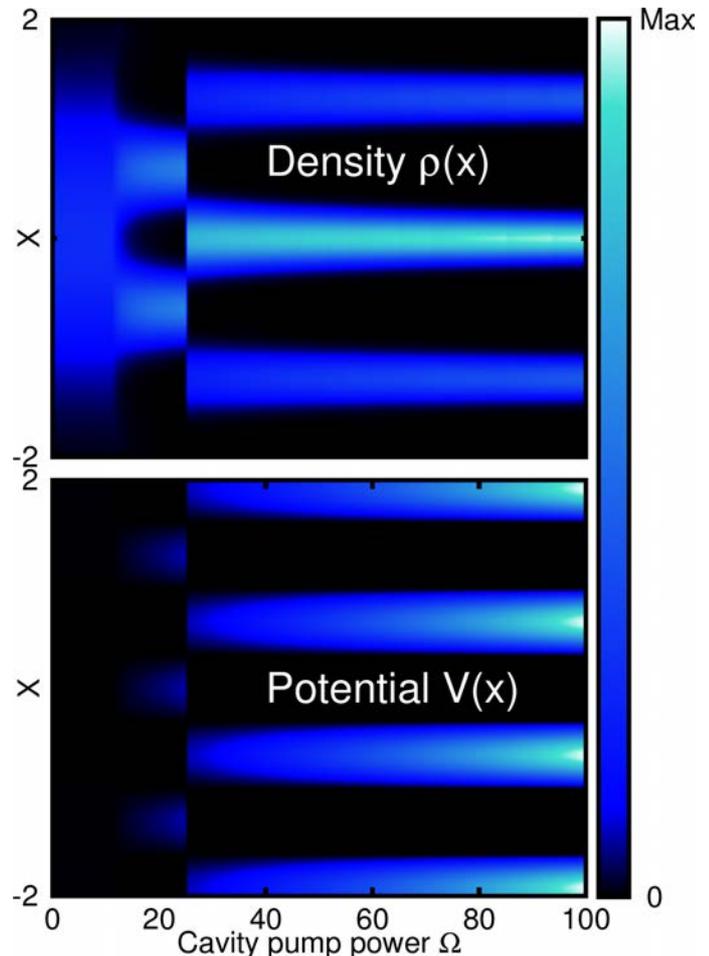

FIG. 2. Self-organization of the ground state of a Bose-Einstein condensate. The density $\rho(x)$ of the atoms and the potential $V(x) = V_{1\text{-body}}(x) + V_{\text{cavity}}(x)$ is shown as a function of the cavity pump power in the upper and lower panels, respectively. Once the applied pump power exceeds a critical value, the atoms self-organize because the field which is built up inside the cavity creates a periodic one-body potential (cf. lower and upper panels). As a result of a competition between external and cavity potential as well as interactions, the sign of the cavity amplitude switches one time for $\Omega \approx 25$ [compare pattern in density and potential with the inset of Fig. 3(a)]. All quantities shown are dimensionless, see text for further discussion.

as a function of the cavity pump power in Fig. 2. Beyond the critical pump power Ω_{cr}, the cavity population $|\alpha|^2$ rises, see Fig. 3(a), and is roughly proportional to the magnitude of the maxima of the potential shown in the lower panel of Fig. 2. The density becomes *self-organized* and the atoms cluster around the minima of the cavity-photon-mediated potential V_{cavity} (compare upper and lower panel in Fig. 2) instead of the minimum of the parabolic confinement $V_{1\text{-body}}(x)$. This self-organization of the atoms marks the transition to the superradiant phase of the Dicke model [15, 16]. The emergent density resembles the density of atoms in optical lattices.
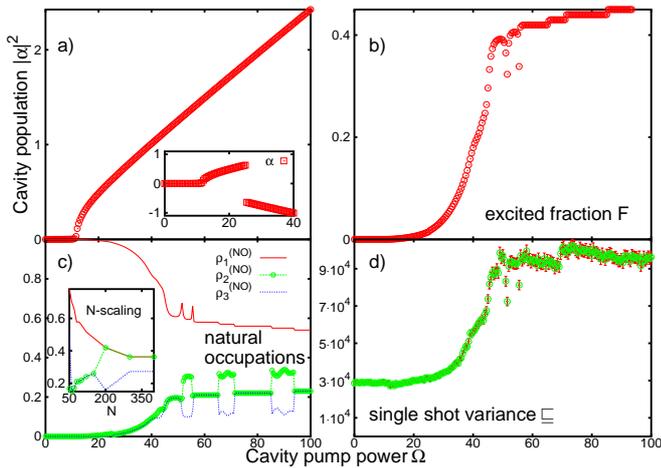
FIG. 3. (a) Buildup of cavity population in the self-organization process. Beyond the critical value $\Omega_{cr} \approx 12$ the population of photons in the cavity grows with increasing pump power Ω. The cavity population $|\alpha|^2$ drives the self-organization of the atoms, see Eq. (3). Inset: The amplitude α shows a sign changes in the superradiant phase at $\Omega \approx 25$ and is monotonous in the fragmented superradiant phase. (b) Fraction F of atoms that are outside the natural orbital with the largest occupation, (c) Natural orbital occupations, and (d) Variance $\mathcal{V}$ in single shots of the momentum density (1000 samples per data point), all as a function of the pump power Ω. The variance $\mathcal{V}$ maps the fraction F of atoms in excited orbitals closely, compare panels (b) and (d). The natural occupations (c) show that the dips in the excited fraction F and the variance are due to a re-distribution of atoms between excited orbitals. The inset of (c) demonstrates that fragmented superradiance emerges for a range of particle numbers N with a finite-size scaling for $\Omega = 80$. The emergence of fragmentation and the growth of F signals that the system enters a new phase with many-body correlations between the atoms. This is confirmed by comparing (b) and (c) with Fig. 4 (a)–(c). All quantities shown are dimensionless, see text.

To assess if correlations between the atoms are built up in their self-organization process, we investigate the cavity population and fragmentation of the system as a function of the cavity pump power. We quantify the fragmentation using the fraction F of atoms which do not occupy the lowest eigenstate of the reduced one-body density matrix

$$\rho^{(1)}(x, x') = \sum_k \rho_k^{(NO)} \phi_k^{(NO),*}(x) \phi_k^{(NO)}(x') . \quad (4)$$

The eigenvalues $\rho_k^{(NO)}$ and eigenfunctions $\phi_k^{(NO)}(x)$ of $\rho^{(1)}$ are known as natural occupations and natural orbitals, respectively [superscript (NO)]. If $\rho^{(1)}$ has only a single macroscopic eigenvalue, $F = 0$, the corresponding system is referred to as condensed. If, on the contrary, $\rho^{(1)}$ has multiple macroscopic eigenvalues, $F > 0$, the corresponding system is referred to as fragmented [31–33]. Figures 3(b) and (c) show a plot of the excited fraction F and the eigenvalues $\rho_k^{(NO)}$, respectively. At

pump powers $\Omega \gtrsim 40 > \Omega_{cr}$, i.e., well into the super-radiant regime, the system fragments. This transition to fragmentation indicates the emergence of correlations and marks the break-down of mean-field approaches like the Gross-Pitaevskii equation, which cannot capture correlations and fragmentation [24, 30]. Furthermore, the simple two-level description of the superradiant system ceases to be applicable for the fragmented superradiant system, see Sec. IV of [37] for details.

The occurrence of this fragmented superradiant phase is one of the main results of our Letter. This result is robust against variations in the particle number as demonstrated by a finite-size scaling plot, see inset in Fig. 3(c). We now discuss how the predicted fragmentation may be detected experimentally. The emergent phase cannot be detected in the photonic part of the system alone, see Fig. 3(a). Its detection requires the simultaneous analysis of the wavefunction of the atoms in the cavity and the cavity photons. We have found that the fragmentation of the Bose-Einstein condensate can be detected in the variance $\mathcal{V}$ of single-shot measurements [37, 49] of the momentum distribution, see Fig. 3(d) for a plot of $\mathcal{V}$. This variance maps the excited fraction of atoms accurately and can therefore be used to assess the fragmentation of the system, compare Figs. 3(b) and (d).

The similarity of the behavior of the excited fraction F and the single-shot variance $\mathcal{V}$ may be understood qualitatively: For a coherent condensate, $F \approx 0$, the variance $\mathcal{V}$ is minimized because all the atoms in the respective single-shot measurements are picked from the same natural orbital. For a fragmented state, $F > 0$, the variance of the single shots grows, since the atoms are picked from a superposition of several mutually orthonormal natural orbitals $\phi_1^{(NO)}$, $\phi_2^{(NO)}$, ... The momenta obtained by drawing from this distribution that lives in a larger space spanned by several orbitals have a wider spread. Hence the variance $\mathcal{V}$ is larger as compared to the values obtained by drawing momenta from a single orbital. We expect that the (momentum-space) variance of single-shot measurements can be used to quantify fragmentation experimentally also in more general setups. Since single-shot measurements require only absorption images, this would mark a clear advantage in comparison to other methods to determine fragmentation that require the measurement of the off-diagonal part of the reduced one-body density matrix [31–33] or density-density correlations [50].

To get a detailed picture of the structure of the emergent many-body correlations, we analyze the spatial correlation function $g^{(1)}(x, x') = \frac{\rho^{(1)}(x,x')}{\sqrt{\rho(x)\rho(x')}}$. For a complementary analysis of the momentum correlation function, see [37]. The correlation function $g^{(1)}$ uses the reduced one-body density matrix $\rho^{(1)}$ to measure the proximity of a many-body state to a product or mean-field state for a given set of coordinates x, x'. It is a key measure for the
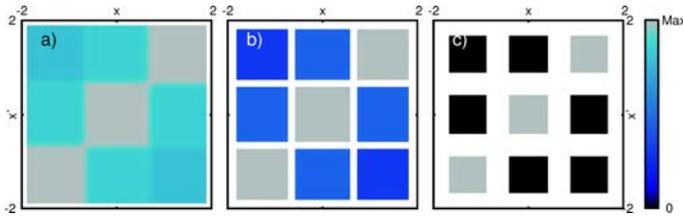
FIG. 4. Tracing the transition from superradiance to fragmented superradiance in the spatial correlation function. The correlation function $|g^{(1)}(x, x')|^2$ in the superradiant phase is shown for pump powers (a) $\Omega = 30$, (b) $\Omega = 40$, and (c) $\Omega = 100$, wherever the density exceeds 0.001. With increasing pump power the atoms in distinct wells gradually loose coherence ($|g^{(1)}(x, x' \neq x)|^2$ drops to zero), compare the position of black squares with the upper panel of Fig. 2. The structure of $|g^{(1)}|^2$ in (c) demonstrates the three-fold fragmentation in the system. All quantities shown are dimensionless.

coherence of ultracold bosonic atoms and experimentally detectable [51, 52]. Figure 4 shows a plot of $|g^{(1)}(x, x')|^2$. The spatial correlation function gives an intuitive picture of the mechanism behind the fragmentation of the system. The potential exerted on the atoms by the photons in the cavity grows with the pump power. Due to the repulsive interparticle interactions the atoms in the distinct wells of this cavity-photon-mediated periodic potential become disconnected beyond a critical magnitude of the pump power. Consequently, the spatial correlation function vanishes gradually for off-diagonal values, see Fig. 4. This observation is consistent with the occurrence of fragmentation, see Figs. 3(b) and (c). The loss of spatial coherence between atoms in distinct wells of the potential generated by the photons in the cavity is complemented by a periodic pattern of correlated and uncorrelated momenta in the momentum correlation function that reflects the periodicity of the potential, see Supplementary Material [37] and Fig. S1 therein.

In conclusion, we have derived and applied a new numerical many-body approach to describe laser-pumped ultracold atoms in cavity fields. We have used the multiconfigurational time-dependent Hartree method for indistinguishable particles, MCTDH-X, to solve the many-body Schrödinger equation of the coupled cavity-atom system. This method self- and size-consistently incorporates correlations between the atoms in the cavity and can also be applied to multi-mode cavities and fermionic atoms.

We have demonstrated that the phase diagram of ultracold bosonic atoms in a single-mode cavity exhibits a fragmented superradiant phase in which the atoms show many-body correlations not captured within two-level or mean-field approaches. While the system remains superradiant, the Bose-Einstein condensate starts to macroscopically occupy multiple single-particle states when the pump power is increased sufficiently. Thus, our work adds a new phase to the phase diagram of bosons in a

cavity which can be detected using the statistics of experimental single shot measurements and the cavity population.

---

* axel.lode@unibas.ch

[1] K. Rzażewski, K. Wódkiewicz, and W. Żakowicz, Phys. Rev. Lett. **35**, 432 (1975).

[2] R. H. Dicke, Phys. Rev. **93**, 99 (1954).

[3] C. Emary and T. Brandes, Phys. Rev. E **67**, 066203 (2003).

[4] H. Ritsch, P. Domokos, F. Brennecke, and T. Esslinger, Rev. Mod. Phys. **85**, 553 (2013).

[5] J. A. Mlynek, A. A. Abdumalikov, C. Eichler, and A. Wallraff, Nature Comm. **5**, 5186 (2014).

[6] M. Feng, Y.P. Zhong, T. Liu, L.L. Yan, W.L. Yang, J. Twamley, and H. Wang, Nature Comm. **6**, 7111 (2015).

[7] O. Viehmann, J. von Delft, and F. Marquardt, Phys. Rev. Lett. **107**, 113602 (2011).

[8] C. Ciuti and P. Nataf, Phys. Rev. Lett. **109**, 179301 (2012).

[9] M. Scheibner, T. Schmidt, L. Worschech, A. Forchel, G. Bacher, T. Passow, and D. Hommel, Nature Phys. **3**, 106 (2007).

[10] D. P. Waters, G. Joshi, M. Kavand, M. E. Limes, H. Malissa, P. L. Burn, J. M. Lupton, and C. Boehme, Nature Phys. **11**, 910 (2015).

[11] H. Xia, A. A. Svidzinsky, L. Yuan, C. Lu, S. Suckewer, and M. O. Scully, Phys. Rev. Lett. **109**, 093604 (2012).

[12] J. G. Bohnet, Z. Chen, J. M. Weiner, D. Meiser, M. J. Holland, and J. K. Thompson, Nature **484**, 78 (2012).

[13] F. Brennecke, R. Mottl, K. Baumann, R. Landig, T. Donner, and T. Esslinger, Proc. Natl. Acad. Sci. **110**, 11763 (2013).

[14] F. Brennecke, T. Donner, S. Ritter, T. Bourdel, M. Köhl, and T. Esslinger, Nature **450**, 268 (2007).

[15] K. Baumann, C. Guerlin, F. Brennecke, and T. Esslinger, Nature **464**, 1301 (2010).

[16] J. Klinder, H. Keler, M. Wolke, L. Mathey, and A. Hemmerich, Proc. Natl. Acad. Sci. **112**, 3290 (2015).

[17] R. Chitra and O. Zilberberg, Phys. Rev. A **92**, 023815 (2015).

[18] M. H. Anderson, J. R. Ensher, M. R. Matthews, C. E. Wiemann, and E. A. Cornell, Science **269**, 198 (1995).

[19] C. C. Bradley, C. A. Sackett, J. J. Tollet, and R. G. Hulet, Phys. Rev. Lett. **75**, 1687 (1995).

[20] K. B. Davis, M.-O. Mewes, M. R. Andrews, N. J. van Druten, D. S. Durfee, D. M. Kurn, and W. Ketterle, Phys. Rev. Lett. **75**, 3969 (1995).

[21] D. Jaksch, C. Bruder, J. I. Cirac, C. W. Gardiner, and P. Zoller, Phys. Rev. Lett. **81**, 3108 (1998).

[22] M. Greiner, O. Mandel, T. Esslinger, T. W. Hänsch, and I. Bloch, Nature **415**, 39 (2002).

[23] E. Fasshauer and A. U. J. Lode, Phys. Rev. A **93**, 033635 (2016).

[24] A. U. J. Lode, K. Sakmann, O. E. Alon, L. S. Cederbaum, and A. I. Streltsov, Phys. Rev. A **86**, 063606 (2012).

[25] D. Nagy, G. Kónya, G. Szirmai, and P. Domokos, Phys. Rev. Lett. **104**, 130401 (2010).

[26] M. Paternostro, G. De Chiara, and G. M. Palma, Phys. Rev. Lett. **104**, 243602 (2010).

[27] C. J. Pethick and H. Smith, *Bose-Einstein Condensation in Dilute Gases* (Cambridge University Press, Cambridge UK, 2002).

[28] L. P. Pitaevskii and S. Stringari, *Bose-Einstein Condensation* (Clarendon Press, Oxford, 2003).

[29] D. Nagy, G. Szirmai, and P. Domokos, Eur. Phys. J. D **48**, 127 (2008).

[30] A. U. J. Lode, *Tunneling Dynamics in Open Ultracold Bosonic Systems*, Springer Theses, Springer, Heidelberg (2014).

[31] R. W. Spekkens and J. E. Sipe, Phys. Rev. A **59**, 3868 (1999).

[32] A. I. Streltsov, O. E. Alon, and L. S. Cederbaum, Phys. Rev. Lett. **99**, 030402 (2007).

[33] P. Bader and U. R. Fischer, Phys. Rev. Lett. **103**, 060402 (2009).

[34] F. Piazza, P. Strack, W. Zwerger, Annals of Physics **339**, 135 (2013).

[35] We first choose a length scale of $L = 1\mu$m. The scale of energy for the mass of ^{87}Rb is $\hbar^2/(mL^2) = 2\pi\hbar \times$ 116Hz, and the scale of time is $mL^2/\hbar = 1.37$ms. The one-dimensional scattering parameter λ_0 is related to the three-dimensional scattering length a_{3D} by $\lambda_0 = 2Lm\omega_\perp a_{3D}/\hbar$ where $\omega_\perp$ is the frequency of the transversal confinement [36]. Using $a_{3D} = 100.4a_0$, where a_0 is the Bohr radius, and $\lambda_0 = 0.01$, one obtains $\omega_\perp = 687.9$Hz.

[36] M. Olshanii, Phys. Rev. Lett. **81**, 938 (1998).

[37] See supplementary material.

[38] H.-D. Meyer, U. Manthe, and L. S. Cederbaum, Chem. Phys. Lett. **165**, 73 (1990); U. Manthe, H.-D. Meyer, and L. S. Cederbaum, J. Chem. Phys. **97**, 3199 (1992).

[39] O. E. Alon, A. I. Streltsov, and L. S. Cederbaum, Phys. Rev. A **77**, 033613 (2008).

[40] O. E. Alon, A. I. Streltsov, and L. S. Cederbaum, J. Chem. Phys. **127**, 154103 (2007).

[41] K. Baumann, *Experimental Realization of the Dicke Quantum Phase Transition*, Ph.D. Thesis No. 19943, ETH Zürich (2012).

[42] O. Penrose and L. Onsager, Phys. Rev. **104**, 576 (1956).

[43] A.U.J. Lode, Phys. Rev. A **93**, 063601 (2016).

[44] A.U.J. Lode, M.C. Tsatsos, and E. Fasshauer, MCTDH-X: *The time-dependent multiconfigurational Hartree method for indistinguishable particles software*, http://ultracold.org.

[45] In the units of Ref. [35], the cavity detuning is $\Delta_c = 43$, the cavity loss rate $\kappa = 11.2$, and the cavity-atom coupling $g_0 = 46$. The cavity and pump mode functions are given by $\cos(k_c x)$, where the k_c-value of the cavity is $k_c = 4.9$.

[46] M. Reza Bakhtiari, A. Hemmerich, H. Ritsch, and M. Thorwart, Phys. Rev. Lett. **114**, 123601 (2015).

[47] R. Landig, L. Hruby, N. Dogra, M. Landini, R. Mottl, T. Donner, and T. Esslinger, Nature **532**, 476 (2016).

[48] Y. Li, L. He, and W. Hofstetter, Phys. Rev. A **87**, 051604 (2013).

[49] K. Sakmann and M. Kasevich, Nature Phys. **12**, 451 (2016).

[50] M. K. Kang and U. R. Fischer, Phys. Rev. Lett. **113**, 140404 (2014).

[51] T. Betz, S. Manz, R. Bücker, T. Berrada, Ch. Koller, G. Kazakov, I.E. Mazets, H.-P. Stimming, A. Perrin, T. Schumm, and J. Schmiedmayer, Phys. Rev. Lett. **106**, 020407 (2011).

[52] A. Perrin, R. Bücker, S. Manz, T. Betz, C. Koller, T. Plisson, T. Schumm, and J. Schmiedmayer, Nature Phys. **8**, 195 (2012).

Supplementary Information

Fragmented superradiance of a Bose-Einstein condensate in an optical cavity

Axel U. J. Lode* and Christoph Bruder

Department of Physics, University of Basel,

Klingelbergstrasse 82, CH-4056 Basel, Switzerland

* axel.lode@unibas.ch

The results of the paper are based on the numerical method described in Sec. I of this supplementary document. In Sec. II we discuss the algorithm used to simulate experimental single-shot measurements, in Sec. III we present calculations of the momentum correlation function that gives additional insights on the build-up of correlations and fragmentation of the condensate, and in Sec. IV we discuss the breakdown of the two-level description in the fragmented superradiant phase.

I.   NUMERICAL METHOD

A.   Hamiltonian

Our goal is to solve the time-dependent many-body Schrödinger equation,

$$i\partial_t |\Psi\rangle = \hat{H} |\Psi\rangle \,, \tag{S1}$$

where $\hat{H}$ is a general Hamiltonian for a system of ultracold atoms which is pumped by a laser and resides in an optical cavity,

$$\hat{H} = \sum_{i=1}^{N} \hat{h}(\vec{r}_i; t) + \sum_{i<j=1}^{N} \hat{W}(\vec{r}_i, \vec{r}_j; t) \,. \tag{S2}$$

Here, $\hat{h}$ is a one-body operator and $\hat{W}$ a two-body interparticle interaction. The potential felt by the atoms created by the cavity photons can be cast in the form of a time-dependent one-body potential $V_{\text{cavity}}(\vec{r}; t)$ and is hence absorbed in the one-body Hamiltonian $\hat{h}$ in Eq. (S2). To compute this cavity-photon potential the equation of motion of the cavity (see below) has to be solved simultaneously and coupled to the many-body problem in Eq. (S1).

B.   MCTDH-X

We use the multiconfigurational time-dependent Hartree method for indistinguishable particles (MCTDH-X) to compute the time-evolution for a general many-body wavefunction

$$|\Psi(t)\rangle = \sum_{\vec{n}} C_{\vec{n}}(t) |\vec{n}; t\rangle \,. \tag{S3}$$

The basis $|\vec{n}; t\rangle$ consists of all possible (anti-)symmetrized products of N particles in M single-particle functions $\{\Phi_i(\vec{r}; t), i = 1, ..., M\}$. This amounts to a description of the atoms

by the field operator $\hat{\Psi}(\vec{r};t) = \sum_{i=1}^{M} \hat{b}_i(t)\Phi_i^*(\vec{r};t)$. The configurations $|\vec{n};t\rangle$ read

$$|\vec{n};t\rangle = \prod_{i=1}^{M} \left[\frac{\left(\hat{b}_i^\dagger(t)\right)^{n_i}}{\sqrt{n_i!}} \right] |vac\rangle . \tag{S4}$$

Applying the time-dependent variational principle to the time-dependent Schrödinger equation with this ansatz while exploiting an invariance property [S1] yields the equations of motion of the MCTDH-X [S2, S3] method:

$$i\partial_t|\Phi_j\rangle = \hat{P}\left[\hat{h}|\Phi_j\rangle + \lambda_0 \sum_{k,s,q,l=1}^{M} \{\boldsymbol{\rho}\}_{jk}^{-1}\rho_{ksql}\hat{W}_{sl}|\Phi_q\rangle\right], \tag{S5}$$

$$i\partial_t\boldsymbol{\mathcal{C}}(t) = \boldsymbol{\mathcal{H}}(t)\boldsymbol{\mathcal{C}}(t), \tag{S6}$$

Eq. (S5) for the orbitals and Eq. (S6) for the coefficients. Here, $\rho_{kq} = \langle\Psi|\hat{b}_k^\dagger\hat{b}_q|\Psi\rangle$ and $\rho_{kqsl} = \langle\Psi|\hat{b}_k^\dagger\hat{b}_s^\dagger\hat{b}_l\hat{b}_q|\Psi\rangle$, are the matrix elements of the reduced one-body and two-body density matrix, respectively. The local interaction potentials $\hat{W}_{sl}(\vec{r}) = \int d\vec{r}'\Phi_s^*(\vec{r}',t)\hat{W}(\vec{r},\vec{r}',t)\Phi_l(\vec{r}',t)$ were introduced, $\boldsymbol{\mathcal{H}}_{\vec{n},\vec{n}'} = \langle\vec{n}';t|\hat{H}|\vec{n};t\rangle$ is the Hamiltonian represented in the chosen many-body basis, and $\boldsymbol{\mathcal{C}}(t)$ is a vector collecting all coefficients $\{C_{\vec{n}}(t)\}$. For the details of the derivation of Eqs. (S5) and (S6), see Refs. [S2, S3].

C. Coupling a many-body system to a multi-mode cavity

In the MCTDH-X equations of motion (Eqs. (S5) and (S6)), the potential exerted on the atoms by the photons in the cavity and the pump was absorbed into the one-body Hamiltonian $\hat{h}$ which retains its form, $\hat{h} = \hat{T}_{\vec{r}} + V(\vec{r};t)$. As mentioned, $\hat{T}_{\vec{r}}$ is the kinetic energy and $V = V_{\text{cavity}}(\vec{r};t) + V_{\text{1-body}}(\vec{r};t)$ the combined external potential of the trapping potential $V_{\text{1-body}}$, the pump laser, and the cavity photons. The potential $V(\vec{r},t)$ is hence modified in a time-dependent way by the interaction of the atoms with the cavity field $\alpha^d(t)$. Here and in the following, the superscript d indexes the cavity modes. The effect of this interaction is two-fold [S4–S6]: the field of the cavity generates a potential $U^d(\vec{r}) = \frac{(g_0^d)^2}{\Delta_a}\left(\xi_C^d(\vec{r})\right)^2$ that contributes to the one-body potential experienced by the atoms and, second, the atoms scatter photons from the pump into the cavity field resulting in a cavity photon source term $\eta^d(\vec{r},t) = \frac{g_0^d\Omega(t)}{\Delta_a}\xi_P(\vec{r})\xi_C^d(\vec{r})$. Here, $\xi_C^d(\vec{r})$ is the profile of the d-th cavity mode, $\xi_P(\vec{r})$ the profile of the pump, g_0^d is the atom-cavity coupling and Δ_a is the detuning of the pump laser from resonance frequency of the atoms. The pump field $V_0(\vec{r};t) = \frac{\Omega^2(t)}{\Delta_a^2}\xi_P^2(\vec{r})$ creates an

3

additional potential for the atoms. Here, the pump Rabi frequency Ω depends on the pump laser power which may be time-dependent. The resulting one-body potential entering the many-body Hamiltonian of bosons in an optical cavity reads

$$V(\vec{r}, t) = V_{\text{1-body}}(\vec{r}, t) + V_0(\vec{r}; t) + \sum_d \left[|\alpha^d(t)|^2 U^d(\vec{r}) + (\alpha^d(t) + \alpha^{*,d}(t))\eta^d(\vec{r}, t) \right],$$

where $V_{\text{1-body}}(\vec{r}, t)$ is the external trapping potential of the system without the cavity and $\xi_P(\vec{r})$ and $\xi_C^d(\vec{r})$ are the pump beam and cavity profiles, respectively. In the one-dimensional setup considered in the main text, the system resides in a node of the pump and therefore there is no contribution of V_0 to the potential. We use the MCTDH-X orbitals (cf. Eq. (S5)) to define the matrix elements $\langle \Phi_k | U^d(\vec{r}; t) | \Phi_q \rangle = U_{kq}^d(t)$ and $\langle \Phi_k | \eta^d(\vec{r}, t) | \Phi_q \rangle = \eta_{kq}^d(t)$, i.e., the expectation values which are necessary to evaluate the equation of motion of the cavity field below. Instead of solving the Master equation that describes photon loss from the cavity, we introduce a complex damping term $-i\kappa^d$ which allows to cast the problem in the form of a set of coupled equations of motion of the cavity populations [S6, S7]:

$$i\partial_t \alpha^d(t) = \left[-\Delta_c^d + \sum_{k,q=1}^M \left(\rho_{kq}(t) U_{kq}^d \right) - i\kappa^d + \sum_{d'} \gamma_{dd'} \alpha^{d',*}(t) \right] \alpha^d(t)$$

$$+ \sum_{k,q=1}^M \left(\rho_{kq}(t) \eta_{kq}^d(t) \right) + \sum_{kq} \left[\rho_{kq} \sum_{d' \neq d} \Gamma_{kq}^{dd'} \alpha^d(t) \alpha^{d',*}(t) \right]. \tag{S7}$$

Here, we used the relations $\langle \Psi(t) | U^d(\vec{r}) | \Psi(t) \rangle = \sum_{k,q=1}^M \left(\rho_{kq}(t) U_{kq}^d \right)$ and $\langle \Psi(t) | \eta^d(\vec{r}, t) | \Psi(t) \rangle = \sum_{k,q=1}^M \left(\rho_{kq}(t) \eta_{kq}^d(t) \right)$. The atom-mediated cavity mode coupling between modes d and d' is given by $\Gamma_{kq}^{dd'} = \nu^{dd'} \langle \phi_k | \xi_C^d(\vec{r}, t) \xi_C^{d'}(\vec{r}, t) | \phi_q \rangle$ with mode coupling constants $\nu^{dd'}$ while the static cavity-mode coupling of mode d and d' is mediated by the coefficients $\gamma_{dd'}$.

Equations (S5), (S6), and (S7) are solved simultaneously to describe the many-body cavity dynamics with MCTDH-X.

Note, that the main text deals with a single-mode cavity for which $\gamma_{dd'} = \Gamma_{kq}^{dd'} = 0$ in Eq. (S7). For the simulations presented in the main text, we used the cavity detuning $\Delta_C = 43$, the cavity loss-rate $\kappa = 11.2$, the cavity-atom coupling $g_0 = 0.46$. The cavity and pump mode functions are given by $\xi_C(x) = \cos(kx) = \xi_P(x)$, where $k = 4.9$. All the cavity parameters are given in the dimensionless units defined in Ref. [35] of the main text.

4

D. Numerical details

We used $M = 3$ orbitals $\Phi_k(\vec{r}; t)$ to represent the many-body state $|\Psi\rangle = \sum_{\vec{n}} C_{\vec{n}} |\vec{n}; t\rangle$. With $N = 100$, this corresponds to $\binom{N+M-1}{N} = 5005$ coefficients $C_{\vec{n}}(t)$. To represent the orbitals, a discrete-variable representation with 1024 plane-wave functions was employed. The grid ranged from -8 to 8.

II.   MEASUREMENT OF FRAGMENTED SUPERRADIANCE WITH SINGLE SHOTS

Here, we show how to simulate experimental single shot measurements from a many-body wavefunction of Bose-Einstein condensed atoms in an optical cavity. To this end, we describe the algorithm to simulate single shots of the many-body wavefunctions (see Ref. [S8] for details) which are the result of computations with MCTDH-X [S9].

A.   Simulation of single shots from many-body wavefunctions

We follow the procedure developed in Ref. [S8] to compute single shots that can be applied both in real ($\vec{r}$-) and momentum ($\vec{k}$-) space. In the following, we present the equations for real space and use $\vec{r}$ for coordinates. To start, we define the N-body wavefunction

$$|\Psi\rangle = \sum_{\vec{n}} C_{\vec{n}} |\vec{n}\rangle. \tag{S8}$$

Here, the index $\vec{n}$ runs through all possible configurations of N bosons in M single-particle states. Consequently the configurations read $|n_1, n_2, ..., n_M\rangle$ with $\sum_k n_k = N$. To simulate a single-shot measurement, we define the probability distribution

$$P(\vec{r}_1, \vec{r}_2, ..., \vec{r}_N) = |\Psi(\vec{r}_1, \vec{r}_2, ..., \vec{r}_N)|^2 \tag{S9}$$

and note that it can be written as a product of conditional probabilities,

$$P(\vec{r}_1, \vec{r}_2, ..., \vec{r}_N) = P(\vec{r}_1)P(\vec{r}_2|\vec{r}_1) \cdots P(\vec{r}_N|\vec{r}_{N-1}, ..., \vec{r}_1). \tag{S10}$$

Here, $P(\vec{r}_a|\vec{r}_b, \vec{r}_c)$ represents the conditional probability to find a particle at $\vec{r}_a$, given that other particles are found at $\vec{r}_b$ and $\vec{r}_c$, and analogously for the higher-order conditional

probabilities. A single-shot measurement means to draw the positions of the N particles in the system from the probability distribution given in Eq. (S9), or, equivalently, from Eq. (S10). In the following we will use Eq. (S10), because its representation requires drawing positions from single-variable conditional distributions and is therefore numerically much less demanding than drawing from the N-variable distribution in Eq. (S9). To calculate the conditional probabilities $P(\cdot|\cdot)$, we introduce the *reduced* states

$$|\Psi^d\rangle = \begin{cases} |\Psi\rangle & \text{for } d = 0 \\ \\ \mathcal{N}_d \hat{\Psi}(\vec{r}_d)|\Psi^{d-1}\rangle & \text{for } 0 < d < N \end{cases} \tag{S11}$$

Here, $\vec{r}_d$ is the position of the drawn particle, and $\mathcal{N}_d$ is a normalization factor. The reduced $(N-d)$ and $(N-d-1)$-particle states for a general many-body state $|\Psi\rangle$ of the form in Eq. (S8) read $|\Psi^d\rangle = \sum_{\vec{n}} C_{\vec{n}}^d |\vec{n}\rangle$ and $|\Psi^{d-1}\rangle = \sum_{\vec{n}} C_{\vec{n}}^{d-1} |\vec{n}\rangle$, respectively. The expansion coefficients obey

$$C_{\vec{n}}^d = \mathcal{N}_d \sum_{k=1}^{M} \Phi_k(\vec{r}_d) C_{\vec{n}^k}^{d-1} \sqrt{n_k + 1}. \tag{S12}$$

Here, $\Phi_k(\vec{r}_d)$ are the single-particle wave functions introduced in Eq. (S5), $\vec{r}_d$ is the position of the drawn particle, and $\vec{n}^k = (n_1, ..., n_k + 1, ..., n_M)$ was introduced. In the following, we will use the reduced wavefunction $|\Psi^d\rangle$, that describes $N - d$ particles to evaluate the conditional probabilities in Eq. (S10). For this purpose, we define the one-body densities that correspond to the reduced wavefunctions:

$$\rho_d(\vec{r}) = \langle \Psi^d | \hat{\Psi}^\dagger(\vec{r}) \hat{\Psi}(\vec{r}) | \Psi^d \rangle \tag{S13}$$

The normalization $\mathcal{N}_d$ in Eq. (S11) is hence $\mathcal{N}_d = \frac{1}{\sqrt{\rho_{d-1}(\vec{r}_d)}}$. To obtain a single-shot measurement, i.e., the positions of all particles $\vec{r}_1, ..., \vec{r}_N$, the first position $\vec{r}_1$ is drawn from $P(\vec{r}) = \rho_0(\vec{r})/N$, the second position $\vec{r}_2$ is drawn from $P(\vec{r}|\vec{r}_1)$, etc.. To obtain the conditional probabilities $P(\vec{r}|\cdot)$, we note that $P(\vec{r}|\vec{r}_1, \vec{r}_2, ..., \vec{r}_d) = \frac{P(\vec{r}, \vec{r}_1, \vec{r}_2, ..., \vec{r}_d)}{P(\vec{r}_d, ..., \vec{r}_1)}$ (cf. Eq. (S10) and Eq. (S11)). Furthermore, note that $P(\vec{r}_d, ..., \vec{r}_1)$ is a constant. Hence, the conditional probability $P(\vec{r}|\vec{r}_d, ..., \vec{r}_1)$ is proportional to the density $\rho_d(\vec{r})$.

To summarize, a single-shot measurement can be simulated as follows: Start by drawing a particle position $\vec{r}_d$ from $\rho_{d-1}(\vec{r})$. Then compute Ψ^d from Ψ^{d-1} using Eqs. (S11) and (S12). By normalization, $\mathcal{N}_d$ is determined. From Ψ^d, the conditional probability $P(\vec{r}|\vec{r}_d, ..., \vec{r}_1)$ is

evaluated by computing the density $\rho_d(\vec{r})$, see Eq. (S13). The next particle position $\vec{r}_{d+1}$ is now drawn from this conditional probability and so forth. These steps are repeated for $d = 1, ..., N - 1$ until all particle positions $\vec{r}_1, ..., \vec{r}_N$ have been drawn. To simulate a single-shot measurement, $\mathcal{B}(\vec{r})$, the positions $\vec{r}_1, ..., \vec{r}_N$ are then convoluted with a point spread function. Following Ref. [S8], we use a Gaussian with a width of three pixels.

B. Fragmented superradiance and the variance of single shots of the momentum distribution

Here, we derive a quantity to assess fragmentation from experimental single-shot measurements. We use the above algorithm to simulate experimental single shots to obtain the variance of single-shot measurements in the phase transition to fragmented superradiance discussed in the main text. Since a one-dimensional system is considered here, we will use k synonymously to $\vec{k}$ in the following. We define the variance of a set of single-shot measurements $\{\mathcal{B}_j(k)\}_{j=1}^{N_{\text{shots}}}$ as follows

$$\mathcal{V} = \int dk \frac{1}{N_{\text{shots}}} \sum_{j=1}^{N_{\text{shots}}} \left[\mathcal{B}_j(k) - \bar{\mathcal{B}}(k) \right]^2 ; \qquad \bar{\mathcal{B}}(k) = \frac{1}{N_{\text{shots}}} \sum_{j=1}^{N_{\text{shots}}} \mathcal{B}_j(k) . \qquad (S14)$$

We plot the momentum space single-shot variance $\mathcal{V}$ in Fig. 4 in the main text. The variance clearly maps the behavior of the fragmentation and may hence be used as a straightforward way to experimentally detect the fragmented superradiant phase from time-of-flight images. The similarity of the behavior of fragmentation F and single-shot variance $\mathcal{V}$ may be understood qualitatively: For a coherent state, $F \approx 0$, the variance $\mathcal{V}$ is minimized because all the particles in the respective single-shot measurements are picked from the same single-particle state ϕ. For a fragmented state, $F > 0$, the variance of the single shots grows, because the particles are picked from a superposition of several mutually orthonormal single-particle states $\phi_1, \phi_2, ...$. The momenta obtained by drawing from this distribution that lives in a larger space spanned by several functions have a wider spread, and hence larger variance $\mathcal{V}$ as compared to the values obtained by drawing momenta from a single function. We speculate that the (momentum space) variance of single shots can be used to quantify fragmentation experimentally in general setups and not only the one considered here and in the main text. Since single shots require only absorption images, this would mark a clear advantage in comparison to other methods to determine fragmentation that necessitate the
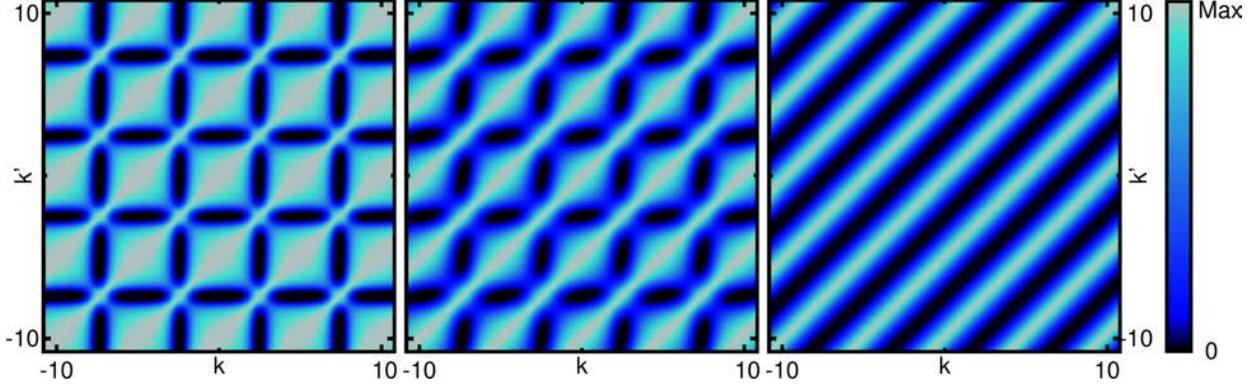
FIG. S1. Tracing the transition from superradiance to fragmented superradiance in the momentum correlation functions of the atoms. The momentum correlation functions $|g^{(1)}(k, k')|^2$ in the superradiant phase are shown for pump-powers $\Omega = 30, 40, 100$ in the left, middle, and right panels, respectively, wherever the momentum density exceeds 0.001. Overall, the momentum correlations are more sensitive to fragmentation than their real-space counterpart (cf. Fig. 4 in the main text): even at the lowest depicted pump rate, $\Omega = 30$, the momentum correlations show a square lattice pattern where $|g^{(1)}|^2 < 1$, although the sample is still almost fully coherent (no fragmentation, $F \approx 0$). Through the transition, the square lattice pattern transforms into a diagonal line pattern of alternating domains of uncorrelated ($|g^{(1)}|^2 \approx 1$) and correlated momenta ($|g^{(1)}|^2 \approx 0$, cf. middle and right panels). All quantities shown are dimensionless.

measurement of correlations [S10] or the off-diagonal part of the reduced one-body density matrix [S11].

III. TRACING THE FRAGMENTED SUPERRADIANT PHASE IN THE MOMENTUM SPACE CORRELATIONS OF THE ATOMS

We now consider the momentum correlations during the transition from superradiance to fragmented superradiance using $g^{(1)}(k, k') = \frac{\rho^{(1)}(k,k')}{\sqrt{\rho(k)\rho(k')}}$, here $\rho^{(1)}(k, k')$ is the reduced one-body density matrix in momentum space. It can be obtained by applying a Fourier transform to the natural orbitals $\phi_k^{(NO)}(x)$ in Eq. (4) in the main text. Figure S1 shows the momentum correlations $|g^{(1)}(k, k')|^2$ as a function of the pump power Ω. The momentum correlations appear to be more susceptible to fragmentation, as they show the loss of coherence already for very small values of the excited fraction F, compare Fig. S1 and Fig. 3(b) of the main

8

text. The pattern of squares that emerges in the transition to fragmented superradiance in the spatial correlations [cf. Fig. 4(a)–(c) of the main text] is visible in the momentum correlations as a periodic structure of diagonal lines of alternating coherent ($|g^{(1)}|^2 \approx 1$) and incoherent ($|g^{(1)}|^2 \approx 0$) momenta, see right panel in Fig. S1.

IV. BREAKDOWN OF THE TWO-LEVEL DESCRIPTION IN MOMENTUM SPACE

Here, we consider the validity of the description of the superradiant state with a two-level picture in momentum space (2LP). We find that the system can be described with the 2LP when it is superradiant and not fragmented. When fragmentation emerges and the system enters the fragmented superradiant phase, however, the 2LP breaks down. To illustrate this behavior, we plot the momentum density $\rho^{(1)}(k,k)$ and the skew-diagonal of the reduced density matrix in momentum space, $\rho^{(1)}(k,-k)$ as a function of the pump power Ω in Fig. S2. With the transition from superradiance to fragmented superradiance, the peaks at $\pm\hbar k_c$ that are the characteristic feature of the momenum distribution $\rho^{(1)}(k,k)$ in the 2LP disappear gradually. This shows the breakdown of the two-level picture for the fragmented superradiant state. In the skew-diagonal, however, a side-peak structure with a $\pm\hbar k_c/2$ spacing starts to form at the transition to fragmented superradiance. This structure maybe understood as an interference phenomenon: bosons that sit in different orbitals of the fragmented Bose-Einstein condensate couple *independently* to the field in the cavity and the respective recoil momenta are superimposed.
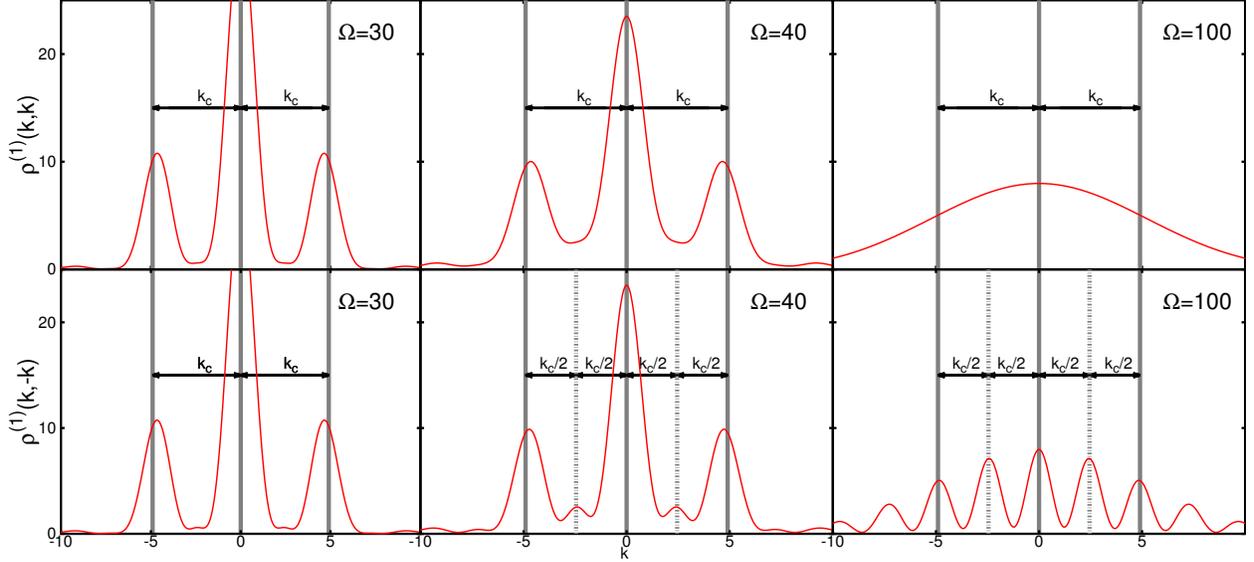
FIG. S2. Emergence of fragmented superradiance and breakdown of the two-level description. The diagonal $\rho^{(1)}(k, k)$ (top) and skew-diagonal $\rho^{(1)}(k, -k)$ (bottom) of the reduced density matrix in momentum space are shown in the superradiant phase for pump powers $\Omega = 30, 40, 100$ in the left, middle, and right column, respectively. In the superradiant but non-fragmented region, two side-peaks are visible at $\pm k_c$, where $k_c = 4.9$ is the quasimomentum of the periodic potential spontaneously generated by the cavity photons (top and bottom left). This is as expected from the two-level picture. The side-peaks in the density $\rho^{(1)}(k, k)$ are gradually transformed to a broad single-maximum momentum distribution (top middle and right) indicating the breakdown of the two-level description in momentum space. The skew-diagonal $\rho^{(1)}(k, -k)$ shows the transition to fragmentation; the side-peak structure is transformed from a $\pm k_c$ to a $\pm k_c/2$ spacing. All quantities shown are dimensionless, see text for further discussion.

10

[S1] H.-D. Meyer, U. Manthe, and L. S. Cederbaum, The multi-configurational time-dependent Hartree approach, Chem. Phys. Lett. **165**, 73 (1990); U. Manthe, H.-D. Meyer, and L. S. Cederbaum, Wave-packet dynamics within the multiconfiguration Hartree framework: General aspects and application to NOCl, J. Chem. Phys. **97**, 3199 (1992).

[S2] O. E. Alon, A. I. Streltsov, and L. S. Cederbaum, Multiconfigurational time-dependent Hartree method for bosons: Many-body dynamics of bosonic systems, Phys. Rev. A **77**, 033613 (2008).

[S3] O. E. Alon, A. I. Streltsov, and L. S. Cederbaum, Unified view on multiconfigurational time propagation for systems consisting of identical particles, J. Chem. Phys. **127**, 154103 (2007).

[S4] K. Baumann, C. Guerlin, F. Brennecke, and T. Esslinger, Dicke quantum phase transition with a superfluid gas in an optical cavity, Nature **464**, 1301 (2010).

[S5] J. Klinder, H. Keler, M. Wolke, L. Mathey, and A. Hemmerich, Dynamical phase transition in the open Dicke model, Proc. Natl. Acad. Sci. **112**, 3290 (2015).

[S6] K. Baumann, Experimental Realization of the Dicke Quantum Phase Transition, Ph.D. Thesis No. 19943, ETH Zürich (2012).

[S7] D. Nagy, G. Szirmai, and P. Domokos, Self-organization of a Bose-Einstein condensate in an optical cavity, Eur. Phys. J. D **48**, 127 (2008).

[S8] K. Sakmann and M. Kasevich, Nature Phys. **12**, 451 (2016).

[S9] A. U. J. Lode, M. C. Tsatsos, and E. Fasshauer MCTDH-X: *The time-dependent multiconfigurational Hartree method for indistinguishable particles software*, http://ultracold.org.

[S10] M. K. Kang and U. R. Fischer, Revealing Single-Trap Condensate Fragmentation by Measuring Density-Density Correlations after Time of Flight, Phys. Rev. Lett. **113**, 140404 (2014).

[S11] O. Penrose and L. Onsager, Bose-Einstein Condensation and Liquid Helium, Phys. Rev. **104**, 576 (1956).